Charge Transfer Interaction of Intermolecular Hydrogen Bonds in 7-Azaindole(MeOH)$_n$ (n = 1, 2) with IR-Dip Spectroscopy and Natural Bond Orbital Analysis

Yutaka Kageura, Kenji Sakota, and Hiroshi Sekiya*

Department of Chemistry, Faculty of Sciences and Department of Molecular Chemistry, Graduate School of Science, Kyushu University, 6-10-1 Hakozaki, Higashi-ku, Fukuoka 812-8581, Japan

Received: March 3, 2009; Revised Manuscript Received: May 7, 2009

Resonance-enhanced two-photon ionization (RE2PI) spectra of the deuterated 7-azaindole [7AI](MeOH)$_n$ (n = 1−3) clusters in the 0−0 region of the S_1-S_0 ($\pi\pi^*$) transition and IR−UV ion-dip spectra of the deuterated 7AI(MeOH)$_n$ (n = 1, 2) in the NH and OH stretch regions are observed in the gas phase to investigate the effect of charge transfer delocalization interaction on intermolecular hydrogen bonds. Two and three isotopomers are identified for 7AI(MeOH)$_1$-d_1 and 7AI(MeOH)$_2$-d_2, respectively, where 7AI(MeOH)$_1$-d_1 has a deuterium atom in the NH or OH group and 7AI(MeOH)$_2$-d_2 has two deuterium atoms in the NH and OH groups or in the two OH groups. The local modes of the NH and OH groups are successfully observed in the IR-dip spectra upon deuteration. The NH and OH stretch fundamentals of the 7AI(MeOH)$_1$-d_1 and 7AI(MeOH)$_2$-d_2 clusters are red-shifted from the corresponding ones of the 7AI and MeOH monomers. The observed red-shifts in 7AI(MeOH)$_1$-d_1 and 7AI(MeOH)$_2$-d_2 are correlated with the second-order perturbative energies obtained by the natural bond orbital analysis, suggesting that the charge transfer delocalization interaction plays an important role in stabilizing the intermolecular hydrogen bonds in 7AI(MeOH)$_n$ (n = 1, 2).

1. Introduction

Hydrogen-bonding (H-bonding) interaction is one of the most important intra- and intermolecular interactions in molecules, clusters, and supramolecular systems to determine their geometries, reactivities, and functions.[1−4] A unique feature of the H-bond is a directional interaction. The directional interaction of the H-bond plays a crucial role for the formation of the secondary and tertiary structures of proteins in the folding processes.[5] Recently, it is proposed that the partial unfolding−folding conversion of the protein structure induces the allosteric conformational change of adenylate kinase and the stepping motions in motor protein.[6,7] H-bond interaction, which is related to unfolding−folding conversions of protein structures, may control the flexible response of supramolecular systems such as proteins to generate their functions.

The origin of H-bonding interaction has been explained from two different points of view so far.[2,3] One is an electrostatic interaction such as a dipole−dipole interaction, and the other is a covalent type interaction. Covalent type interaction can be regarded as charge transfer interaction from the proton-accepting molecules to the proton-donating molecules.[8−10] Energy decomposition schemes, where the interaction energy is decomposed into components of electrostatic and covalent type (charge transfer) interactions, were applied for a number of H-bonded systems.[11−14] For example, strong H-bonds such as $[F-H-F]^-$ are explained by covalent type interaction, while weak H-bonds such as CH···O are explained by electrostatic interaction.[3,9] Previous studies indicated that the component of covalent type interaction may increase when H-bond strength becomes strong.[9,15] It should be mentioned that H-bonding energy cannot be decomposed experimentally into the two components.

The red-shift measurements of the fundamentals of the vibrational mode that is associated with the H-bonds provide very useful information about H-bonding interaction.[16−19] However, the coupling of H-bonded modes prevents clear analysis of the observed red-shift. For example, H-bonded stretch local modes couple with each other to form normal modes. When the normal mode is very different from the local mode, the red-shifts of the vibrational fundamentals of the normal modes cannot directly correlate with the H-bond strengths in each H-bonding site. The deuteration of the H-bonded hydrogen is an excellent method to quench the coupling of the H-bonded NH and OH stretch modes in order to correlate the red-shifts of the vibrational fundamentals with the H-bond strengths.

Cooperativity is one of the most intriguing features in H-bonded networks, where an H-bond is strengthened by forming another H-bond at different H-bonding sites.[2,3,20−24] Theoretical calculations pointed out that the cooperativity of the H-bond plays a significant role for stabilizing the secondary structures of proteins.[25−33] Very recently, we reported the IR−UV ion-dip (IR-dip) spectra of supersonically jet-cooled 7-azaindole(MeOH)$_n$ (n = 1−3) clusters [7AI(MeOH)$_n$ (n = 1−3)] in the S_0 state.[34] It was shown that 7AI(MeOH)$_{1-3}$ have cyclic H-bonded structures, where the NH group and the heteroaromatic N atom in 7AI act as the proton donor and the proton acceptor, respectively. The comparison of the experimentally observed red-shifts of the H-bonded OH stretching fundamentals in 7AI(MeOH)$_{2,3}$ and the corresponding one in (MeOH)$_2$ revealed that the OH···O H bond in 7AI(MeOH)$_{2,3}$ is cooperatively enhanced by forming H-bonds at proximal H-bonding sites. The mechanism of the cooperative enhancement in 7AI(MeOH)$_{2,3}$ was investigated by the natural bond orbital (NBO) analysis, which well explained the H-bonding interaction as the donor−acceptor charge transfer delocalization between the lone pair orbitals in the proton acceptor and the antibonding orbital in the proton donor.[8,10]

In the present paper, we report the resonance-enhanced two-photon ionization (RE2PI) spectra of deuterated 7AI(MeOH)$_n$ (n = 1−3) in the 0−0 region of the $S_1-S_0(\pi\pi^*)$ transition and the IR-dip spectra of deuterated 7AI(MeOH)$_n$ (n = 1, 2) in the H-bonded NH and OH stretch regions. We have observed the

* Corresponding author. E-mail: sekiya@chem.kyushu-univ.jp.

10.1021/jp9019377 CCC: $40.75
Published on Web 06/04/2009

NH and OH stretch modes of partially deuterated 7AI(MeOH)$_{1,2}$. These modes can be regarded as the local modes for a good approximation. The H-bond strengths in each H-bonding site could be quantitatively discussed on the basis of the red-shifts of the NH and OH stretch local modes of 7AI(MeOH)$_{1,2}$ from the corresponding NH and OH stretch modes of 7AI and MeOH monomers. We show that there is a good linear correlation between the observed red-shifts of the NH and the OH stretch local modes of 7AI(MeOH)$_{1,2}$ with the second-order perturbative energies obtained by the NBO analysis. The role of the charge transfer interaction in stabilizing the H-bonds has been discussed.

2. Experimental and Computational Section

2.1. Experimental Details. 7AI, undeuterated MeOH, and deuterated MeOH were purchased from TCI, Wako, and Aldrich Co. Ltd., respectively. These reagents were used without further purification. 7AI was introduced into a stainless tube and heated to 353 K by a coiled heater. The Ne carrier gas passes through a reservoir containing the undeuterated and/or deuterated MeOH. The vaporized 7AI was mixed with the undeuterated MeOH and/or the deuterated MeOH and expanded into the vacuum chamber by mixing with the carrier gas. The isotopomers having the ND or OD group in 7AI(MeOH)$_1$ are designated as 7AI(MeOH)$_1$-d_1 and those having the ND and OD groups or two OD groups in 7AI(MeOH)$_2$ as 7AI(MeOH)$_2$-d_2. The backing pressure in the nozzle housing was 3 atm. A pulsed valve (General Valve, series 9, 0.5 mm diameter) was operated at 10 Hz. The RE2PI and IR-dip spectra were measured with a differentially pumped linear time-of-flight (TOF) mass spectrometer. For the RE2PI and IR-dip experiments, a frequency-doubled dye-laser (Sirah Cobra stretch) pumped by a second harmonic of the Nd^{3+}:YAG laser (Spectra Physics GCR 230) was operated at 10 Hz, which was used as a UV source. A typical laser power was 200−500 μJ/pulse. An optical parametric converter (LaserVision) pumped by an injection-seeded Nd^{3+}:YAG laser (Continuum Powerlite Precision II 8000) was operated at 5 Hz, which was used as an IR source. The laser power was typically 1−2 mJ/pulse. The UV and IR pulses were focused with $f = 300$ mm focal lenses. In the RE2PI experiment, a tightly focused UV pulse was introduced at a right angle to the molecular beam. The ion signal generated by the UV pulse was detected by z-stack microchannel plates and amplified by a preamplifier (SRS SR445A). The parent mass signal was detected by using a mass gate. The signal was digitized by the digital oscilloscope (LeCroy Waverunner 64Xi) and fed into the PC for further analysis. In the IR-dip experiment, two pulses were counter-propagated and introduced into a vacuum chamber. The IR beam was typically defocused to 10−30 mm from a tightly focused position to avoid saturation of the absorption in the IR-dip spectrum. The UV pulse was delayed by 20−30 ns with respect to the IR pulse with a digital delayed pulse generator (SRS DG535). The ion signals generated by the UV plus IR pulses and the UV pulse were averaged separately. Each data sequence was recorded in the PC as a function of the IR frequency. The intensities of the ion signals due to the UV plus IR pulses were divided by the intensities of the ion signals induced by the UV pulse to eliminate long-term fluctuations of the baseline.

2.2. Computational Details. Second-order Møller−Plesset perturbative theory (MP2) calculations were performed to obtain the stable structures in the potential energy minima, harmonic vibrational frequencies, and IR intensities in the S_0 state of 7AI(MeOH)$_1$-d_1 and 7AI(MeOH)$_2$-d_2 with the 6-31++G** basis sets for the H-bonded hydrogen (or deuterium) atoms and all nitrogen and oxygen atoms, while using the 6-31G* basis sets for the other atoms. The calculated harmonic vibrational frequencies were scaled by 0.9439. The scaling factor was determined by comparing the calculated and experimentally observed NH stretch fundamentals of the 7-azaindole monomer. The NBO analyses for 7AI(CH$_3$OH)$_n$ ($n = 1, 2$) were made by B3LYP/6-31++G**/6-31G* for the stable structures obtained by MP2 calculations to obtain the second-order perturbative energies. All calculations were performed by using a GAUSSIAN 03 program package.[35] The computation was carried out using the computer facilities at the Research Institute for Information Technology, Kyushu University.

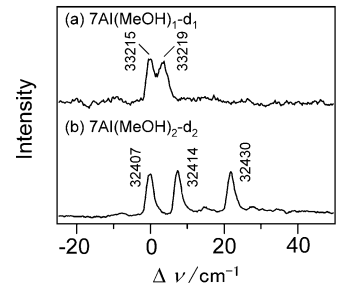

Figure 1. (a) RE2PI spectrum of 7AI(MeOH)$_1$-d_1. Two origin bands are identified at 33 215 and 33 219 cm^{-1}. (b) RE2PI spectra of 7AI(MeOH)$_2$-d_2. Three origin bands are identified at 32 407, 32 414, and 32 430 cm^{-1}. These origins arise from isotopomers, which are deuterated at different H-bonding sites (see Section 3.1). The abscissa indicates the relative wavenumber from the lowest energy origin bands in the two spectra.

3. Results and Discussion

3.1. RE2PI Spectra of Deuterated 7AI(MeOH)$_n$ (n = 1−3). Parts a and b of Figure 1 show the RE2PI spectra of 7AI(MeOH)$_1$-d_1 and 7AI(MeOH)$_2$-d_2, respectively, where d_1 and d_2 indicate the number of the deuterium atoms in each cluster. In Figure 1a, a partially overlapped strong transition is observed, where two peaks are detected at 33 215 and 33 219 cm^{-1}. These two peaks are blue-shifted by 12 and 16 cm^{-1}, respectively, from the 0−0 transition of 7AI(MeOH)$_1$-d_0, where d_0 indicates the undeuterated 7AI(MeOH)$_1$ cluster. In the case of the deuterated 7AI(H$_2$O)$_1$ clusters, the blue-shifting peaks were also identified in the RE2PI spectra.[36] In 7AI(MeOH)$_1$, the hydrogen atoms in the NH and OH groups are preferentially deuterated. Therefore the two peaks must be isotopomers of 7AI(MeOH)$_1$-d_1 that have ND/OH or NH/OD groups. We distinguish two isotopomers having the ND/OH and NH/OD groups with notations 7AI(MeOH)$_1$-[ND] and 7AI(MeOH)$_1$-[OD], respectively.

The two isotopomers have different electronic transition energies originating from different zero-point energies. The NH(ND) and OH(OD) stretch vibrations have larger contributions to the zero-point energies of the two isotopomers than the other modes. The blue-shifts of the 0−0 transitions of the two isotopomers relative to that of 7AI(MeOH)$_1$-d_0 could be correlated with the differences in wavenumbers of the NH and OH stretch vibrations in S_0 and S_1. The large blue-shift of the S_1-S_0 (0−0) transition may originate from the deuteration of the H-bonded group that shows a large difference in the vibrational wavenumbers in S_0 and S_1. We infer that the difference in the vibrational wavenumbers in S_0 and S_1 is larger for the NH stretch vibration than for the OH stretch vibration, because the $\pi\pi^*$ electronic transition occurs in the 7AI moiety. Therefore, the S_1-S_0 (0−0) transitions at 33 219 cm^{-1} and 33 215 cm^{-1} are ascribed to 7AI(MeOH)$_1$-[ND] and 7AI(MeOH)$_1$-[OD], respectively.

In Figure 1b, three strong bands are observed at 32407, 32414, and 32430 cm^{-1}, which are blue-shifted by 40, 47, and 63 cm^{-1},

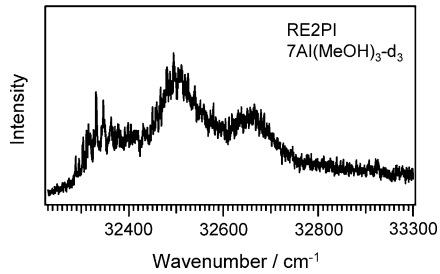

Figure 2. RE2PI spectrum of 7AI(MeOH)$_3$-d_3. The broad spectral feature is due to a spectral congestion of low-frequency intermolecular vibrations (see Section 3.1).

respectively, from the 0−0 transition of 7AI(MeOH)$_2$-d_0. In the previous study, we assigned these three bands to the origin bands of 7AI(MeOH)$_2$-d_2 isotopomers, which have NH/OD(1)/OD(2), ND/OH(1)/OD(2), and ND/OD(1)/OH(2) groups.[37] The labels of OH groups are indicated in Figure 6. Three isotopomers are distinguished with the notations 7AI(MeOH)$_2$-[OD(1)/OD(2)], 7AI(MeOH)$_2$-[ND/OD(2)], and 7AI(MeOH)$_2$-[ND/OD(1)], respectively. We infer that the differences in the vibrational wavenumbers in S_0 and S_1 become larger in order of the stretch vibrations, OH(2) < OH(1) < NH, because the $\pi\pi^*$ electronic excitations are localized in the 7AI moieties. Thus, the 0−0 transitions at 32 407, 32 414, and 32 430 cm^{-1} are ascribed to 7AI(MeOH)$_2$-[OD(1)/OD(2)], 7AI(MeOH)$_2$-[ND/OD(2)], and 7AI(MeOH)$_2$-[ND/OD(1)], respectively.

Figure 2 shows the RE2PI spectrum of 7AI(MeOH)$_3$-d_3 that has three deuterium atoms. This spectrum is fairly broad as compared with those in Figure 1 because of the overlapping of sharp bands in the 32 300−32 350 cm^{-1} region with a broad background in the wide wavenumber region. In the RE2PI spectrum of the undeuterated 7AI(MeOH)$_3$-d_0 cluster, low-frequency vibronic transitions are separately detected, although the spectral pattern is congested.[37,38] There are four isotopomers for 7AI(MeOH)$_3$-d_3, where three different H-bonding sites are deuterated. Therefore, the very broad feature of the spectrum in Figure 2 must be due to the overlap of several vibronic transitions. In ref 34, we reported the IR-dip spectrum of 7AI(MeOH)$_3$-d_0 together with those of 7AI(MeOH)$_{1,2}$-d_0. However, the broad spectral feature in Figure 2 prevents the observation of IR-dip spectra of 7AI(MeOH)$_3$-d_3 obtained by probing the vibronic bands of each isotopomer.

3.2. IR-Dip Spectra and Theoretical Analyses of 7AI(MeOH)$_1$-d_1. Figure 3a shows the IR-dip spectrum of 7AI(MeOH)$_1$-d_0, while parts b and c of Figure 3 are those of 7AI(MeOH)$_1$-[ND] and 7AI(MeOH)$_1$-[OD], respectively, together with the theoretical stick IR spectra of each isotopomer. In the previous study, we assigned the vibrational transition at 3384 cm^{-1} in Figure 3a to the antisymmetric stretch fundamental of the NH and OH groups.[34] This observation is consistent with the cyclic H-bonded structure, where the NH group and N atom in 7AI act as the proton donor and acceptor, respectively. The stable structure does not change by deuterating NH or OH groups under the Born−Oppenheimer approximation because the potential energy surfaces that determine the stable structures do not change by the deuterations. Accordingly the isotopomers 7AI(MeOH)$_1$-[ND] and 7AI(MeOH)$_1$-[OD] have essentially the same cyclic H-bonded structures as the undeuterated one. In Figure 3b, a strong transition is observed at 3367 cm^{-1}, while a strong transition is detected at 3372 cm^{-1} as well as a weak transition at 3391 cm^{-1} in Figure 3c. Theoretical calculations predict the positions of the OH stretch fundamental for 7AI(MeOH)$_1$-[ND] and the NH stretch fundamental for 7AI(MeOH)$_1$-[OD] at 3378 and 3382 cm^{-1}, respectively. These values are in good agreement with the observed fundamentals at 3367 and 3372 cm^{-1}, respectively. Thus, the vibrational transitions at 3367 and 3372 cm^{-1} in Figure 3b,c are assigned to the OH and NH stretch fundamentals of 7AI(MeOH)$_1$-[ND] and 7AI(MeOH)$_1$-[OD], respectively. The weak transition at 3391 cm^{-1} in Figure 3c may be due to the combination or overtone transition originating from the anharmonic coupling.

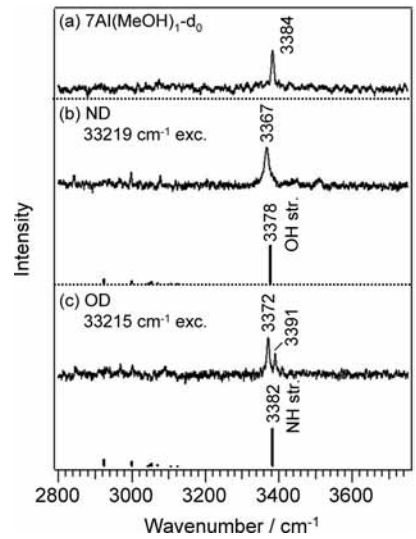

Figure 3. IR-dip and the theoretical stick IR spectra of (b) 7AI(MeOH)$_1$-[ND] probed at 33 219 cm^{-1} and (c) 7AI(MeOH)$_1$-[OD] probed at 33 215 cm^{-1}. The IR-dip spectrum of (a) 7AI(MeOH)$_1$-d_0 is indicated for comparison. The wavenumbers of the strong transitions are indicated in the figure. Notations [OH str.] and [NH str.] indicate the OH stretch vibration in the moiety of MeOH and the NH stretching vibration in the moiety of 7AI, respectively. The vibrational wavenumbers and the transition intensities are calculated at the MP2/6-31++G**/6-31G* level of theory. Calculated wavenumbers are scaled by 0.9439.

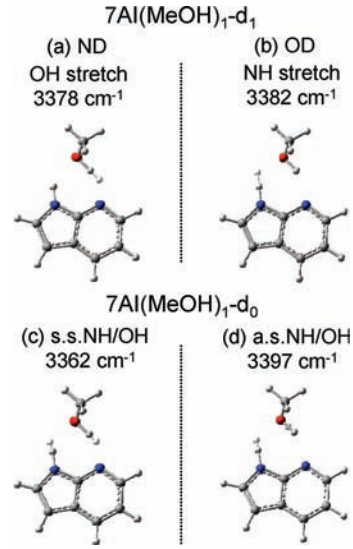

Figure 4. Displacements of the calculated vibrational modes of (a) the OH stretch in 7AI(MeOH)$_1$-[ND], (b) the NH stretch in 7AI(MeOH)$_1$-[OD], and (c and d) the symmetric and antisymmetric stretching in 7AI(MeOH)$_1$-d_0, respectively. The vibrational modes are calculated at the MP2/6-31++G**/6-31G* level of theory.

Figure 4 displays the displacements of the atoms in the calculated vibrational modes of (a) 7AI(MeOH)$_1$-[ND], (b) 7AI(MeOH)$_1$-[OD], and (c and d) 7AI(MeOH)$_1$-d_0. Figure 4c,d shows the symmetric and antisymmetric stretch vibrations of

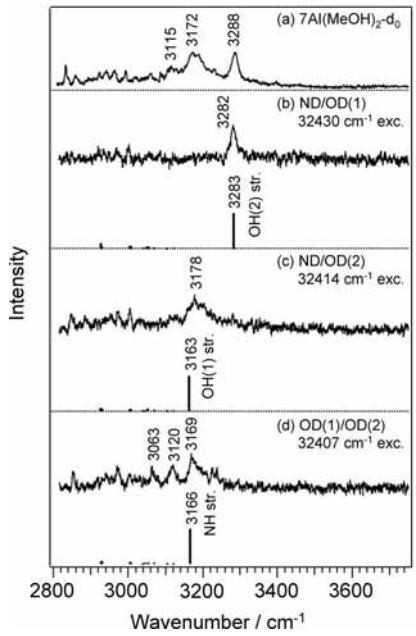

Figure 5. IR-dip and the theoretical stick IR spectra of (b) 7AI-(MeOH)$_2$-[ND/OD(1)] probed at 32 430 cm^{-1}, (c) 7AI(MeOH)$_2$-[ND/OD(2)] probed at 32 414 cm^{-1}, and (d) 7AI(MeOH)$_2$-[OD(1)/OD(2)] probed at 32 407 cm^{-1}. The IR-dip spectrum of (a) 7AI(MeOH)$_2$-d_0 is indicated for comparison. The wavenumbers of the strong transitions are indicated in the figure. The notations [OH(2) str.], [OH(1) str.], and [NH str.] indicate the OH(2) stretch vibration in the moiety of MeOH(2), the OH(1) stretch vibration in the moiety of MeOH(1), and the NH stretch vibration in the moiety of 7AI, respectively. The labeled numbers in parentheses are shown in Figure 6. The vibrational wavenumbers and transition intensities are calculated by MP2/6-31++G**/6-31G*. Calculated wavenumbers are scaled by 0.9439.

the NH and OH groups in 7AI(MeOH)$_1$-d_0. In Figure 4c,d, the displacements of both the NH and the OH hydrogen atoms are prominent. In Figure 4a,b, however, the displacements of the OH hydrogen or NH hydrogen are predominant in 7AI(MeOH)$_1$-[ND] and 7AI(MeOH)$_1$-[OD], respectively. This indicates that the OH or NH stretching mode is almost completely localized because of large differences in the vibrational energies of the deuterated and undeuterated groups. Thus, the coupling between the NH and the OH local modes through intracluster interaction is successfully removed by deuteration.

In Figure 3b,c, ion dips are observed at 3367 and 3372 cm^{-1}, which are assigned to the OH and NH local modes, respectively. The positions of the two bands are very close, suggesting that the energetically quasi-equivalent NH and OH local modes couple with each other and generate the symmetric and antisymmetric stretch vibrations in 7AI(MeOH)$_1$-d_0. It is worth noting that 7AI(MeOH)$_1$-d_0 shows only a single dip at 3384 cm^{-1} although the symmetric and antisymmetric stretch vibrations may exist in the same energy region. The NH and OH local modes have similar vibrational wavenumbers. Therefore, the two modes may couple with nearly the same weights. In addition, the NH and OH groups form antiparallel H-bonds. Thus, the vector differentials of the dipole moments of the 7AI and MeOH moieties, which are proportional to the intensity of the vibrational transition, could be canceled for the symmetric stretch vibration. This idea reasonably explains the disappearance of the symmetric stretch vibration of 7AI(MeOH)$_1$-d_0 in the IR-dip spectrum.

3.3. IR-Dip Spectra and Theoretical Analyses of 7AI-(MeOH)$_2$-d_2. Figure 5a shows the IR-dip spectra of 7AI-(MeOH)$_2$-d_0, while Figure 5b−d is the IR-dip spectra of 7AI(MeOH)$_2$-[ND/OD(1)], 7AI(MeOH)$_2$-[ND/OD(2)], and 7AI-

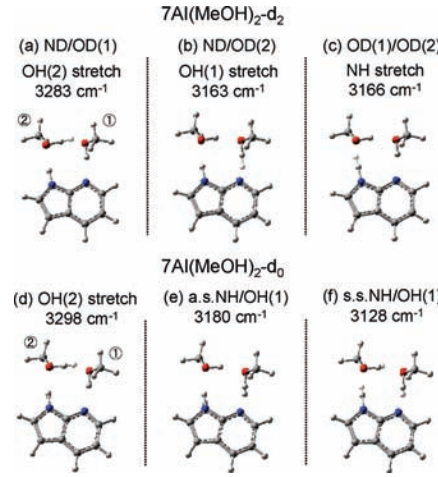

Figure 6. Displacements of the calculated vibrational modes of (a) the OH(2) stretch in 7AI(MeOH)$_2$-[ND/OH(1)], (b) the OH(1) stretch in 7AI(MeOH)$_2$-[ND/OD(2)], (c) the NH stretch in 7AI(MeOH)$_2$-[OD(1)/OD(2)], and (c−e) the OH(2), antisymmetric and symmetric stretch in 7AI(MeOH)$_2$-d_0, respectively. The vibrational modes are calculated at the MP2/6-31++G**/6-31G* level of theory.

(MeOH)$_2$-[OD(1)/OD(2)], respectively, together with the theoretical stick IR spectra for each isotopomer. In the previous study, we assigned the vibrational bands at 3288, 3172, and 3115 cm^{-1} in Figure 5a to the OH(2) stretch fundamental and the antisymmetric and symmetric stretch fundamentals of the NH and OH(1) groups, respectively.[34] The labels of the OH groups in the MeOH moieties are indicated in Figure 6. In Figure 5b,c, prominent bands are observed at 3282 and 3178 cm^{-1}, respectively. In Figure 5d, three bands are detected at 3169, 3120, and 3063 cm^{-1} in the 3000−3200 cm^{-1} region. The theoretical calculations predict the positions of the OH(2), OH(1), and NH stretch fundamentals of 7AI(MeOH)$_2$-[ND/OD(1)], 7AI(MeOH)$_2$-[ND/OD(2)], and 7AI(MeOH)$_2$-[OD(1)/OD(2)] at 3283, 3163, and 3166 cm^{-1}, respectively. The predicted wavenumbers are in good agreement with the observed ones. Thus, we assigned the transitions observed at 3282, 3178, and 3169 cm^{-1} to the OH(2), OH(1), and NH stretch fundamentals of 7AI(MeOH)$_2$-[ND/OD(1)], 7AI(MeOH)$_2$-[ND/OD(2)], and 7AI(MeOH)$_2$-[OD(1)/OD(2)], respectively. The spectral feature in Figure 5d is significantly different from those in Figure 5b,c; three bands with moderate intensities are detected at 3169, 3120, and 3063 cm^{-1} in Figure 5d, but only one band is strong in Figure 5b,c. Theoretical calculations predict the positions of the NH bend vibrations at 1495 and 1560 cm^{-1} for 7AI(MeOH)$_2$-[OD(1)/OD(2)]. Thus, the bands at 3120 and 3063 cm^{-1} in Figure 5d may be due to Fermi resonances between the NH stretch fundamental and the overtone of the NH bend modes.

Figure 6 shows the displacements of the atoms in the calculated vibrational modes of (a) 7AI(MeOH)$_2$-[ND/OD(1)], (b) 7AI(MeOH)$_2$-[ND/OD(2)], (c) 7AI(MeOH)$_2$-[OD(1)/OD(2)], and (d−f) 7AI(MeOH)$_2$-d_0, respectively. The effects of deuteration on the normal modes are clear when we compare the displacements of the NH and/or OH hydrogen atoms among Figure 6a,d, Figure 6b,e, and Figure 6c,f. In Figure 6a−c, the displacements of the vibrational modes are localized in the moieties of the OH(2) group, the OH(1) group, and the NH group, respectively. The localization must be caused by the decoupling of the deuterated groups with the NH or OH groups, because the difference in the vibrational energies between the deuterated and the undeuterated groups is large. In Figure 6e,f, the NH and OH(1) groups show the antisymmetric and

TABLE 1: Summary of Observed Wavenumbers, Assignments, Red-Shifts from the NH and OH Stretch Fundamentals of 7AI and MeOH Monomers, the $E_{i\rightarrow j^*}^{(2)}$ Energies in Each H-Bonding Site in Units of kcal/mol, and the Elongation of the NH and OH Bond Lengths (Δr) from Those of the 7AI and MeOH Monomers

	observed wavenumber, cm^{-1}	assignment	red-shift from NH str. (7AI) or OH str. (MeOH),[a] cm^{-1}	$E_{i\rightarrow j^*}^{(2)}$[b]	Δr, Å[c]
			7AI(MeOH)$_1$-d_1		
ND	3367	OH str.	−315	15.48 (OH···N)	0.016
OD	3372	NH str.	−149	7.44 (NH···O)	0.009
			7AI(MeOH)$_2$-d_2		
ND/OD(1)	3282	OH(2) str.	−400	23.09 (OH(2)···O(1))	0.022
ND/OD(2)	3178	OH(1) str.	−504	26.85 (OH(1)···N)	0.027
OD(1)/OD(2)	3169	NH str.	−352	20.54 (NH···O(2))	0.020

[a] The wavenumbers of the NH and OH stretching vibrations in 7AI and MeOH monomers were observed at 3521 cm^{-1} and 3682 cm^{-1} in refs 39 and 40. [b] From ref 34. [c] Elongation of the NH and OH bond lengths from those of 7AI and MeOH monomer. These values were obtained from calculations at the MP2/6-31++G**/6-31G* level.

symmetric stretch vibrations that correspond to the out-of-phase and in-phase NH and OH(1) stretch vibrations. Such motions may occur because of quasi-equivalent vibrational energies of the NH and OH(1) local modes. This explanation is consistent with the decoupling of the NH and OH groups upon deuteration.

In the previous study, we pointed out that the OH(2) stretch fundamental of 7AI(MeOH)$_2$-d_0 at 3288 cm^{-1} is remarkably red-shifted from the corresponding fundamental of (MeOH)$_2$ by 286 cm^{-1}.[34] This indicates that the OH(2)···O(1) H-bond strength is cooperatively enhanced by forming the NH···O(2) and OH(1)···N H-bonds. In the case of 7AI(MeOH)$_2$-d_0, however, the theoretical IR spectrum in Figure 6d shows that the 3288 cm^{-1} mode involves small displacements of the NH and OH(1) groups. The coupling between the two groups cannot be ignored, but it is difficult to separate the contributions of the NH and OH(1) groups to the observed red-shift in 7AI(MeOH)$_2$-d_0. However, it is clear from Figure 6a that the coupling of the NH and OH(1) groups is removed. The OH(2) stretching fundamental of 7AI(MeOH)$_2$-[ND/OH(1)] is red-shifted from the corresponding fundamental of (MeOH)$_2$ by 292 cm^{-1}, which is close to the value of 7AI(MeOH)$_2$-d_0.

3.4. Role of Charge Transfer Interaction in the H-Bond. The experimentally observed red-shifts of the stretch vibrations of the H-bonded groups include information about the H-bond strengths. However, the coupling of the motions of the groups associated with the H-bonds makes the analyses of the H-bond strengths from the experimental red-shifts difficult. The observation of the local modes through the deuteration of the NH and/or OH groups enabled us to extract clear information about the individual H-bond strengths on the basis of the observed red-shifts for 7AI(MeOH)$_1$-d_1 and 7AI(MeOH)$_2$-d_2 from the corresponding fundamentals of the NH and OH stretch in the 7AI and MeOH monomers.

Table 1 summarizes the observed wavenumbers of the local stretch fundamentals, the red-shifts from the corresponding fundamentals of the NH and OH stretch of the 7AI and MeOH monomers, the second-order perturbative energies ($E_{i\rightarrow j^*}^{(2)}$) for individual H-bonding sites obtained by NBO,[34] and the elongation of the H-bonded NH and OH bond lengths (Δr) of the 7AI(MeOH)$_1$-d_1 and 7AI(MeOH)$_2$-d_2 clusters from the corresponding ones of the 7AI and MeOH monomers. The wavenumbers of the NH and OH stretch fundamentals of 7AI and MeOH were reported to be at 3521 and 3682 cm^{-1}, respectively.[39,40] It should be noted that the deuterations of the NH and OH groups have no effect on the $E_{i\rightarrow j^*}^{(2)}$ energies. In 7AI(MeOH)$_1$-d_1, the red-shift of the OH stretch fundamental is more than twice larger than that of the NH stretch fundamental. Thus, the OH···N H-bond strength is stronger than the NH···O H-bond strength. In 7AI(MeOH)$_2$-d_2, the red-shifts of the OH and NH stretch fundamentals from the corresponding fundamentals of each monomer are larger in the order of NH < OH(2) < OH(1). Therefore, the H-bond strengths become stronger in the order of NH···O < OH(2)···O < OH(1)···N in 7AI(MeOH)$_2$-d_2. Figure 7 shows plots of the elongation of the H-bonded NH and OH bond lengths (Δr) in 7AI(MeOH)$_1$-d_1 and 7AI(MeOH)$_2$-d_2 against the observed red-shifts of the OH and NH stretching fundamentals of 7AI(MeOH)$_1$-d_1 and 7AI(MeOH)$_2$-d_2. The elongation of the bond lengths of the H-bonded NH and OH groups becomes prominent with increasing the red-shifts of the NH and OH stretch fundamentals, which is in accordance with the relative H-bond strengths discussed above.

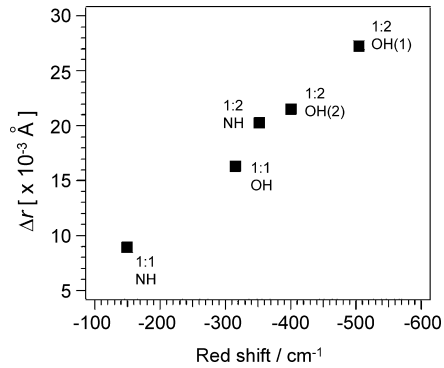

Figure 7. Plots of the observed red-shifts of the NH and OH stretch local modes of 7AI(MeOH)$_1$-d_1 and 7AI(MeOH)$_2$-d_2 from the corresponding NH and OH stretch modes of the 7AI and MeOH monomers versus the elongation of the H-bonded NH and OH bond lengths (Δr) of 7AI(MeOH)$_1$-d_1 and 7AI(MeOH)$_2$-d_2 from the corresponding ones of the 7AI and MeOH monomers. The Δr values in units of 10^{-3} Å are obtained from calculations at the MP2/6-31++G**/6-31G* level.

The NBO model explains the H-bonding interaction as the proton donor−acceptor charge transfer delocalization.[8,10] The lowering of the energy caused by the H-bonding interaction can be estimated by the second-order perturbative energy $E_{i\rightarrow j^*}^{(2)}$. The $E_{i\rightarrow j^*}^{(2)}$ energies reflect the charge transfer interaction in the individual H-bond sites. Figure 8 shows plots of the $E_{i\rightarrow j^*}^{(2)}$ energies against the observed red-shifts of the OH and NH stretching fundamentals of 7AI(MeOH)$_1$-d_1 and 7AI(MeOH)$_2$-d_2. The number of data (five points) plotted in Figure 8 may be insufficient from the statistical point of view. However, Figure 8 clearly shows a tendency that the red-shifts of the stretching fundamentals of the H-bonded groups nicely correlate with the strength of the charge transfer interaction; the $E_{i\rightarrow j^*}^{(2)}$ energy increases with increasing the red-shifts of the OH and NH stretch fundamentals. This finding indicates that the covalent nature becomes important with increasing the strength of the H-bond, because the H-bond has a nature of partial covalency because of the charge transfer interaction.[8−10] It should be mentioned that the above argument does not imply that the charge transfer

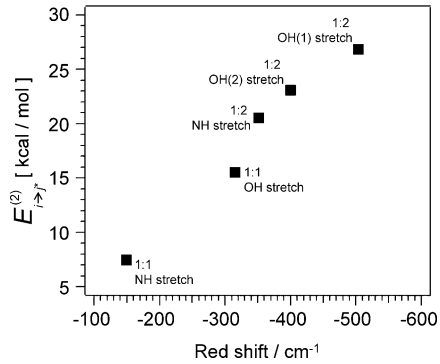

Figure 8. Plots of the observed red-shifts of the NH and OH stretch local modes in 7AI(MeOH)$_1$-d_1 and 7AI(MeOH)$_2$-d_2 from the corresponding NH and OH stretch modes in 7AI and MeOH monomers versus the second-order perturbative energies, $E^{(2)}_{i-j^*}$, obtained by NBO.

interaction (the covalent nature) is the dominant interaction in H-bonds of 7AI(MeOH)$_1$-d_1 and 7AI(MeOH)$_2$-d_2. In the case of the moderate H-bond strengths investigated in this study, the dominant interaction may be the electrostatic interaction.[3,9] However, the contribution of the charge transfer interaction (the covalent nature) becomes important with increasing the strength of the intermolecular H-bonds in the 7AI(MeOH)$_{1,2}$ clusters.

4. Conclusions

We have investigated the H-bonding interactions in 7AI(MeOH)$_n$ ($n = 1-3$) in the gas phase by measuring the IR-dip spectra and NBO analysis in the previous study. The combination of the observed red-shifts of the vibrational modes of the H-bonded group with NBO analysis provides very useful information about H-bonding interactions. However, the coupling of the H-bonded groups prevents direct correlation between the red-shifts and the second-order perturbative energies obtained by NBO analysis. Partial deuteration of the H-bonded NH and OH groups has been successfully applied to correlate the spectral red-shifts of 7AI(MeOH)$_1$-d_1 and 7AI(MeOH)$_2$-d_2 from the 7AI and MeOH monomers with the second-order perturbative energies.

We obtained the relative H-bond strengths in each H-bonding site of 7AI(MeOH)$_1$-d_1 and 7AI(MeOH)$_2$-d_2 on the basis of the experimentally observed red-shifts of the local stretching fundamentals of 7AI(MeOH)$_1$-d_1 and 7AI(MeOH)$_2$-d_2 from the corresponding ones of the NH stretch in 7AI and the OH stretch in MeOH. The H-bond strengths become larger in the order of OH$\cdots$N < NH$\cdots$O in 7AI(MeOH)$_1$-d_1 and NH$\cdots$O < OH(2)$\cdots$O < OH(1)$\cdots$N in 7AI(MeOH)$_2$-d_2. It has been found that the red-shifts of the local stretching vibrations of 7AI(MeOH)$_1$-d_1 and 7AI(MeOH)$_2$-d_2 show a correlation with the second-order perturbative energies, $E^{(2)}_{i-j^*}$, obtained by the NBO analyses. This relationship shows that the charge transfer interaction plays an important role in the H-bonding interactions in 7AI(MeOH)$_n$ ($n = 1, 2$).

Acknowledgment. The authors thank Dr. Yoshiteru Matsumoto at the University of Hyogo for valuable discussions. This work was partly supported by the Grants-in-Aid for Young Scientists B (20750014) and Scientific Research B (20350011) and the Grant-in-Aid for Scientific Research in Priority Area (461) "Molecular Theory for Real Systems" (No. 19029034) and (477) "Molecular Science for Supra Functional Systems - Development of Advanced Methods for Exploring Elementary Processes" (19056005) from the Japanese Ministry of Education, Sports, Science and Technology (MEXT).

References and Notes

(1) Jeffrey, G. A.; Saenger, W. *Hydrogen bonding in biological structures*; Springer-Verlag: New York, 1991.
(2) Scheiner, S. *Hydrogen bonding: A theoretical perspective*; Oxford University Press: New York, 1997.
(3) Jeffrey, G. A. *An introduction to hydrogen bonding*; Oxford University Press: New York, 1997.
(4) Desiraju, G. R.; Steiner, T. *The weak hydrogen bond: In structural chemistry and biology*; Oxford University Press: New York, 1999.
(5) Lodish, H.; Berk, A.; Matsudaira, P.; Kaiser, C. A.; Krieger, M.; Scott, M. P.; Zipurski, L.; Darnell, J. W. H. *Molecular cell biology*; Freeman & Co.: New York, 2004.
(6) Miyashita, O.; Onuchic, J. N.; Wolynes, P. G. *Proc. Natl. Acad. Sci. U.S.A.* **2003**, *100*, 12570.
(7) Terada, T. P.; Sasai, M.; Yomo, T. *Proc. Natl. Acad. Sci. U.S.A.* **2002**, *99*, 9202.
(8) Reed, A. E.; Curtiss, L. A.; Weinhold, F. *Chem. Rev.* **1988**, *88*, 899.
(9) Desiraju, G. R. *Acc. Chem. Res.* **2002**, *35*, 565.
(10) Weinhold, F.; Landis, C. *Valency and Bonding*; Cambridge University Press: New York, 2005.
(11) Kitaura, K.; Morokuma, K. *Int. J. Quantum Chem.* **1976**, *10*, 325.
(12) Stevens, W. J.; Fink, W. H. *Chem. Phys. Lett.* **1987**, *139*, 15.
(13) Sokalski, W. A.; Roszak, S.; Pecul, K. *Chem. Phys. Lett.* **1988**, *153*, 153.
(14) Glendening, E. D.; Streitwieser, A. *J. Chem. Phys.* **1994**, *100*, 2900.
(15) Grabowski, S. J.; Sokalski, W. A.; Dyguda, E.; Leszezynski, J. *J. Phys. Chem. B* **2006**, *110*, 6444.
(16) Zwier, T. S. *Annu. Rev. Phys. Chem.* **1996**, *47*, 205.
(17) Ebata, T.; Fujii, A.; Mikami, N. *Int. Rev. Phys. Chem.* **1998**, *17*, 331.
(18) Brutschy, B. *Chem. Rev.* **2000**, *100*, 3999.
(19) Matsuda, Y.; Mikami, N.; Fujii, A. *Phys. Chem. Chem. Phys.* **2009**, *11*, 1279.
(20) Del Bene, J.; Pople, J. A. *Chem. Phys. Lett.* **1969**, *4*, 426.
(21) Mo, O.; Yanez, M.; Elguero, J. *J. Chem. Phys.* **1992**, *97*, 6628.
(22) Kar, T.; Scheiner, S. *J. Phys. Chem. A* **2004**, *108*, 9161.
(23) Ziolkowski, M.; Grabowski, S. J.; Leszezynski, J. *J. Phys. Chem. A* **2006**, *110*, 6514.
(24) Grabowski, S. J.; Leszezynski, J. *Chem. Phys.* **2009**, *355*, 169.
(25) Hinton, J. F.; Harpool, R. D. *J. Am. Chem. Soc.* **1977**, *99*, 349.
(26) Sheridan, R. P.; Lee, R. H.; Peters, N.; Allen, L. C. *Biopolymers* **1979**, *18*, 2451.
(27) Kobko, N.; Dannenberg, J. J. *J. Phys. Chem. A* **2003**, *107*, 10389.
(28) Ireta, J.; Neugebauer, J.; Scheffler, M.; Rojo, A.; Galvan, M. *J. Phys. Chem. B* **2003**, *107*, 1432.
(29) Wieczorek, R.; Dannenberg, J. J. *J. Am. Chem. Soc.* **2003**, *125*, 8124.
(30) Wieczorek, R.; Dannenberg, J. J. *J. Am. Chem. Soc.* **2003**, *125*, 14065.
(31) Kobko, N.; Dannenberg, J. J. *J. Phys. Chem. A* **2003**, *107*, 6688.
(32) Chen, Y. F.; Dannenberg, J. J. *J. Am. Chem. Soc.* **2006**, *128*, 8100.
(33) Chen, Y. F.; Viswanathan, R.; Dannenberg, J. J. *J. Phys. Chem. B* **2007**, *111*, 8329.
(34) Sakota, K.; Kageura, Y.; Sekiya, H. *J. Chem. Phys.* **2008**, *129*, 054303.
(35) Frisch, M. J.; Trucks, G. W.; Schlegel, H. B.; Scuseria, G. E.; Robb, M. A.; Cheeseman, J. R.; Montgomery, J. A., Jr.; Vreven, T.; Kudin, K. N.; Burant, J. C.; Millam, J. M.; Iyengar, S. S.; Tomasi, J.; Barone, V.; Mennucci, B.; Cossi, M.; Scalmani, G.; Rega, N.; Petersson, G. A.; Nakatsuji, H.; Hada, M.; Ehara, M.; Toyota, K.; Fukuda, R.; Hasegawa, J.; Ishida, M.; Nakajima, T.; Honda, Y.; Kitao, O.; Nakai, H.; Klene, M.; Li, X.; Knox, J. E.; Hratchian, H. P.; Cross, J. B.; Bakken, V.; Adamo, C.; Jaramillo, J.; Gomperts, R.; Stratmann, R. E.; Yazyev, O.; Austin, A. J.; Cammi, R.; Pomelli, C.; Ochterski, J. W.; Ayala, P. Y.; Morokuma, K.; Voth, G. A.; Salvador, P.; Dannenberg, J. J.; Zakrzewski, V. G.; Dapprich, S.; Daniels, A. D.; Strain, M. C.; Farkas, O.; Malick, D. K.; Rabuck, A. D.; Raghavachari, K.; Foresman, J. B.; Ortiz, J. V.; Cui, Q.; Baboul, A. G.; Clifford, S.; Cioslowski, J.; Stefanov, B. B.; Liu, G.; Liashenko, A.; Piskorz, P.; Komaromi, I.; Martin, R. L.; Fox, D. J.; Keith, T.; Al-Laham, M. A.; Peng, C. Y.; Nanayakkara, A.; Challacombe, M.; Gill, P. M. W.; Johnson, B.; Chen, W.; Wong, M. W.; Gonzalez, C.; Pople, J. A. *Gaussian 03*, Revision D.02; Gaussian, Inc.: Wallingford, CT, 2004.
(36) Kim, S. K.; Bernstein, E. R. *J. Phys. Chem.* **1990**, *94*, 3531.
(37) Sakota, K.; Inoue, N.; Komoto, Y.; Sekiya, H. *J. Phys. Chem. A* **2007**, *111*, 4596.
(38) Sakota, K.; Komoto, Y.; Nakagaki, M.; Ishikawa, W.; Sekiya, H. *Chem. Phys. Lett.* **2007**, *435*, 1.
(39) Yokoyama, H.; Watanabe, H.; Omi, T.; Ishiuchi, S.; Fujii, M. *J. Phys. Chem. A* **2001**, *105*, 9366.
(40) Halonen, L. *J. Chem. Phys.* **1997**, *106*, 7931.

JP9019377